Supporting Information for manuscript titled:

'Super-resolution fluorescence microscopy study of the production of K1 capsules by *Escherichia coli: evidence for the differential distribution of the capsule at the poles and the equator of the cell*'

Sorasak Phanphak[i], Pantelis Georgiades[i], Ruiheng Li[i], Jane King[ii], Ian S. Roberts[ii□], Thomas A. Waigh[i,iii*].

[i] School of Physics and Astronomy, Schuster Building, The University of Manchester, Oxford Road, M13 9PL, UK.

[ii] Faculty of Biology, Medicine and Health, Michael Smith Building, The University of Manchester, Dover street, M13 9PL, UK.

[iii] Photon Science Institute, The University of Manchester, Oxford Road, M13 9PL, UK.

□ i.s.roberts@manchester.ac.uk

*t.a.waigh@manchester.ac.uk

Number of pages: 8

Number of supplementary figures: 6

1. Super-resolution images of encapsulated K1 *E. coli*, EV36 strain

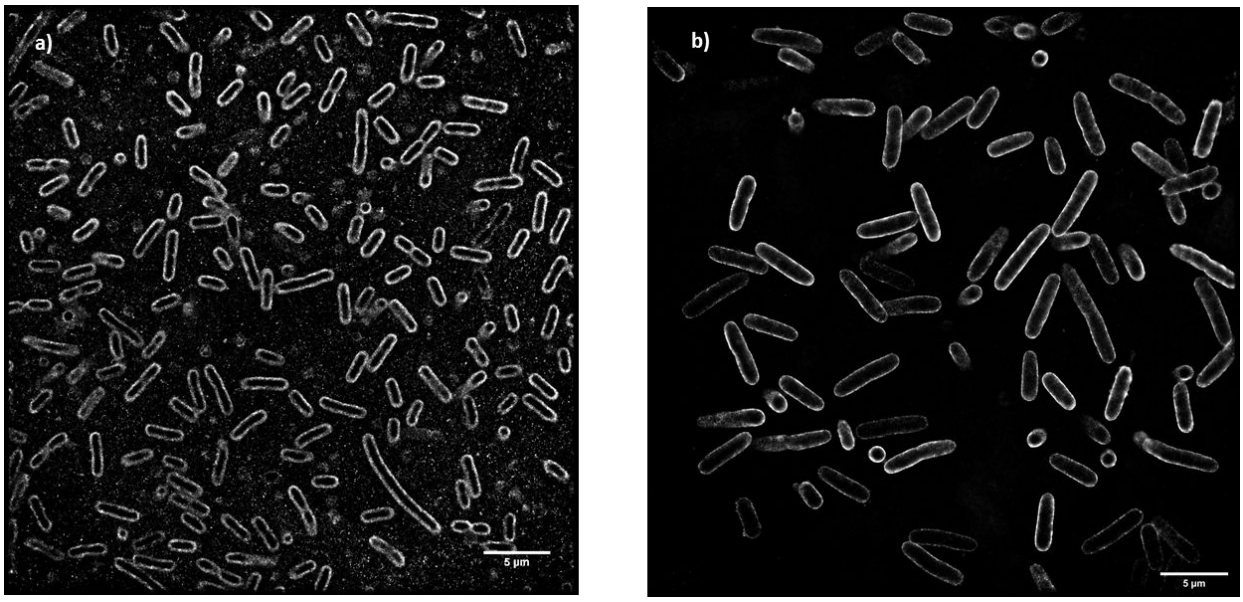

Figure S1. Examples of wide-field super-resolution images of live *E. coli* bacteria, The capsular structures were labelled with anti-K1 conjugated with anti-mouse-AF647 placed in imaging buffer and M9 media. The images were created using dSTORM[1] (50 nm resolution) with PLLGO coated coverslips at different focal planes. **a)** Shows example data used for the analysis of capsular brush thicknesses and their polydispersity. **b)** Shows bacterial cross-sectioning at a level above their mid-point and we omitted this type of image for capsule thickness measurement to avoid projection artefacts. The scale bars are 5 μm.

Examples of wide-field super-resolution images are shown in **figure S1**. High resolution images (50 nm) could be obtained of the capsular structures of a large number of bacteria. The bacteria used for the quantitative thickness calculations were imaged at their mid-points (**figure S1a**) and bacteria were analysed in their more common side on orientation. Other projections in the images, such as end on orientations and slices significantly beyond their midpoints (**figure S1b**) were omitted from the analysis.

2. Calibration of axial projection in super-resolution images using virtual light sheet software to approximate the depth of focus

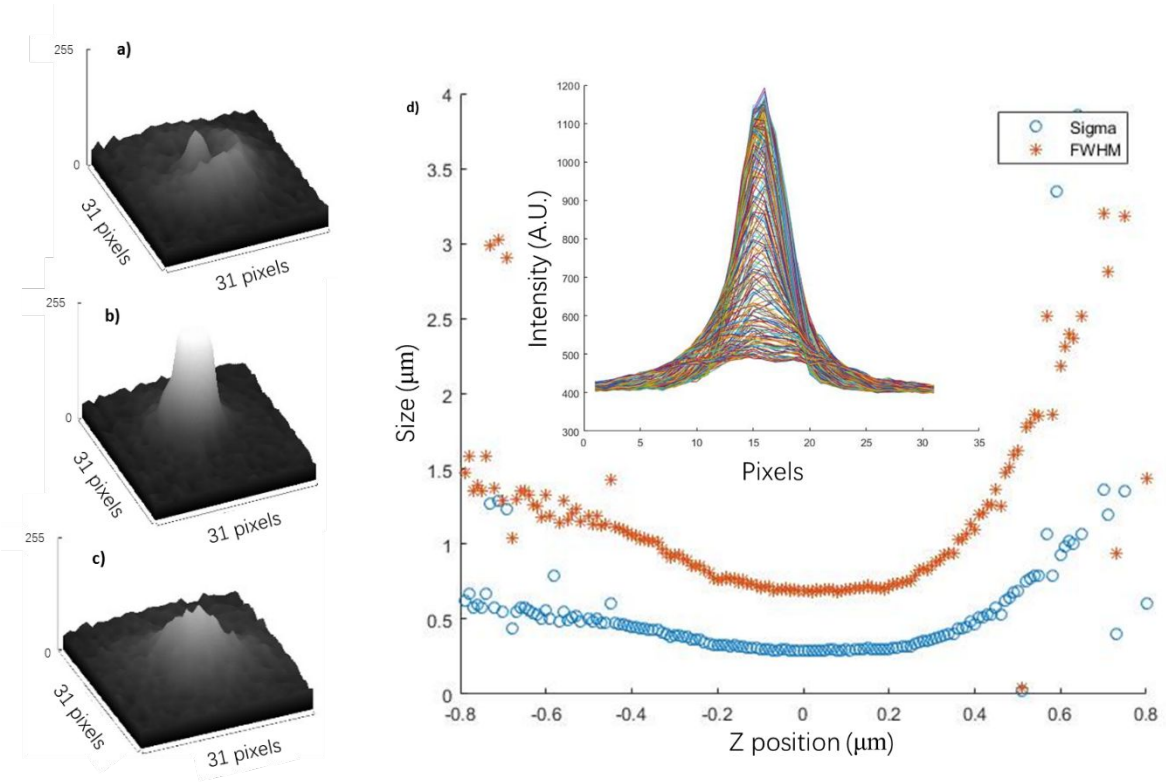

Figure S2. Axial projection calibration using 100 nm polystyrene beads coated in Cy3b for z-stack scans with the super-resolution microscope. **a)**, **b)** and **c)** Show plots of the point spread function (PSF) with positions at *z* = -0.8, 0, and 0.8 µm. **d)** The FWHM and standard deviations (sigma) of Gaussian fits to the data shown in the inset. The inset shows the profiles from all 200 steps of the *z* scan image stack.

The depth of focus (DOF) of our super-resolution microscope was analysed using a virtual light sheet software package[2] and it was found to be 347 ± 22 nm. We used this DOF to quantify its effects on the bacterial capsule thickness measurements and it was found to be negligible e.g. on the results shown in **figure 3**.

3. The calculation of steric forces of the K1 capsule

Consider the osmotic brush model of Pincus for the conformation of polyelectrolyte brushs[3]. When considered at low salt concentration, e.g. less than 10 mM, it is found that:

$$H \cong Na(2ad^2c_s)^{-1/3} . \qquad \text{(S1)}$$

Using the assumption that the highly negative charged polymers experienced strong charge screening, we can characterise the conformation and thickness of capsular polysaccharide using the osmotic pressure model to describe the thicknesses and forces experienced by the lyso-PG brushes, in which the chains are highly strecthed. Hence the thickness of capsular polysaccharide brush can be approximated, by using a grafting length $d \approx 1$ nm[4], a degree of polymerization $N \approx 200$[5,6], a Kuhn length (a) of 1 nm[7], and a salt concentration of around a few 10 mM due to monovalent salt in the M9 media. The brush thickness is found using equation (S1) in the range $H \approx 200 - 300$ nm, which is in reasonable agreement with the measurements from STORM images.

4. The forces experienced by bacterial capsular brushes observed using AFM with spherical probes

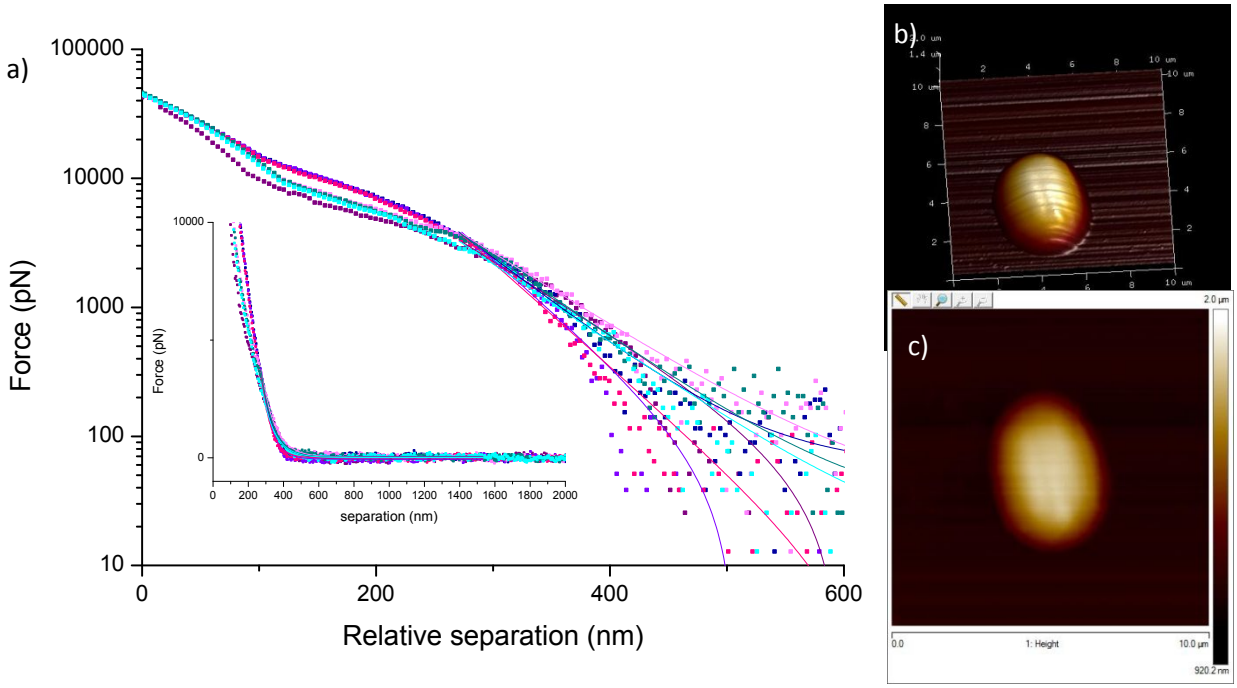

Figure S3. **a)** Force as a function of separation distance from AFM for live encapsulated K1 *E.coli* under hydrated conditions, with filtered miliQ water. The force was fitted with an exponential decay to determine the contact points of the probe with the bacterium (coloured curves). **b)** and **c)** are 3D and 2D images respectively of encapsulated bacteria using AFM scanning with a 2.5 µm spherical probe.

Force curves were obtained for a wide range of bacteria at points on their equators (**figure S2**). Images could be made of bacteria using AFM (**figures S3b**, **S3c**), but this

is a nonspecific imaging technique, so the presence of the capsules could only be determined from the force curves (**figure S3a**).

5. Effect of the oxygen scavenger system with the imaging buffer on bacterial proliferation

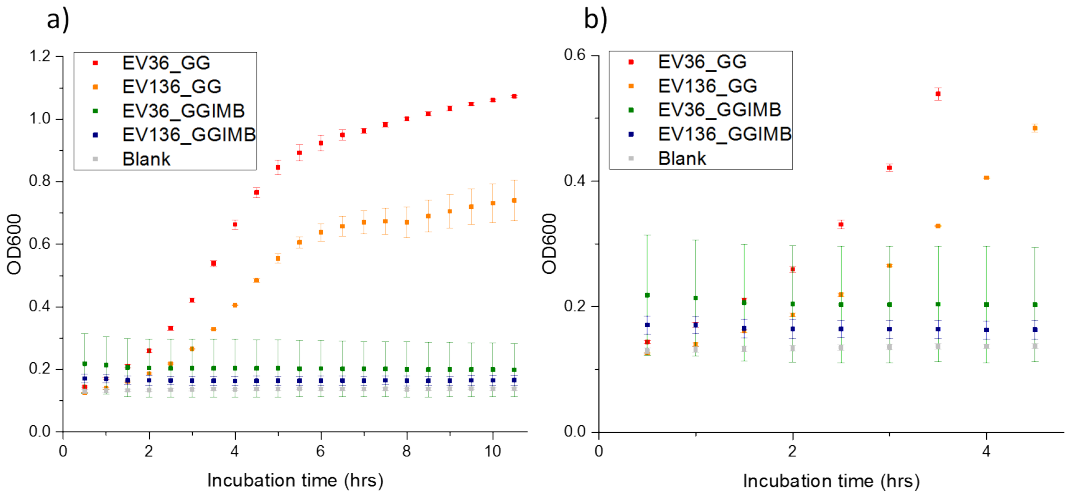

Figure S4. Growth curve of E. coli bacteria (EV36-wild type and EV136-capsule mutant strains) showing OD600 as a function of incubation time with different carbon sources in the growth media. **a)** and **b)** are the same data plotted over different times. The media abbreviations are GG is 0.4% Glucose and 0.4% Glycerol, GGIMB is 0.4% Glucose and 0.4% Glycerol with imaging buffer, and blank is a control media without bacteria. The imaging buffer (IMB) has a significant impact on bacterial proliferation after 2 hours.

Figure S4 shows that the imaging buffer with the oxygen scavenger did perturb the growth of bacterial cells and reduced the population of the bacteria cells over time. However, to circumvent this problem in super-resolution microscopy, we first deposited a high density of bacteria cells on the PLGO coated substrate and then changed the media including the imaging buffer and the M9 media with the carbon source supplement every 1 hour[8]. This allowed us to observe the expansion of capsular lyso-PG raft over 3 hours (the time scale of capsule growth) with no significant artefacts.

6. Effect of the poly-L-lysine coated graphene oxide coverslips on bacterial proliferation.

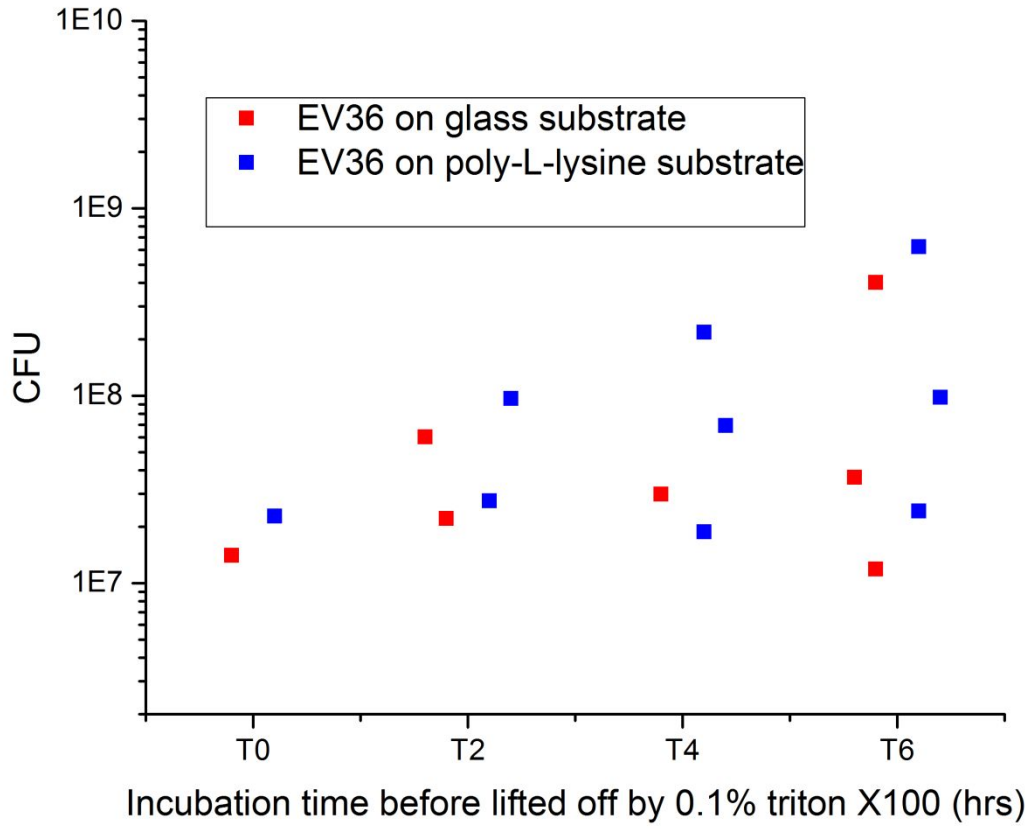

Figure S5. The effect of positive charge substrate (poly-L-lysine) on bacterial growth. Bacteria were grown on the substrate without poly-L-lysine coated (red) and with poly-L-lysine coated (blue) from 0 to 6hrs. Then the deposited cells were lifted off using 0.1% triton X100 and grown on a culture plate to perform a viable count.

The proliferation of bacteria was also examined in contact with poly-L-lysine coatings (**figure S5**). No significant changes were observed over the time scales of our experiments (3 hours) compared with the glass substrate control.

7. The protein machines involved in the production of K1 polysaccharide capsules

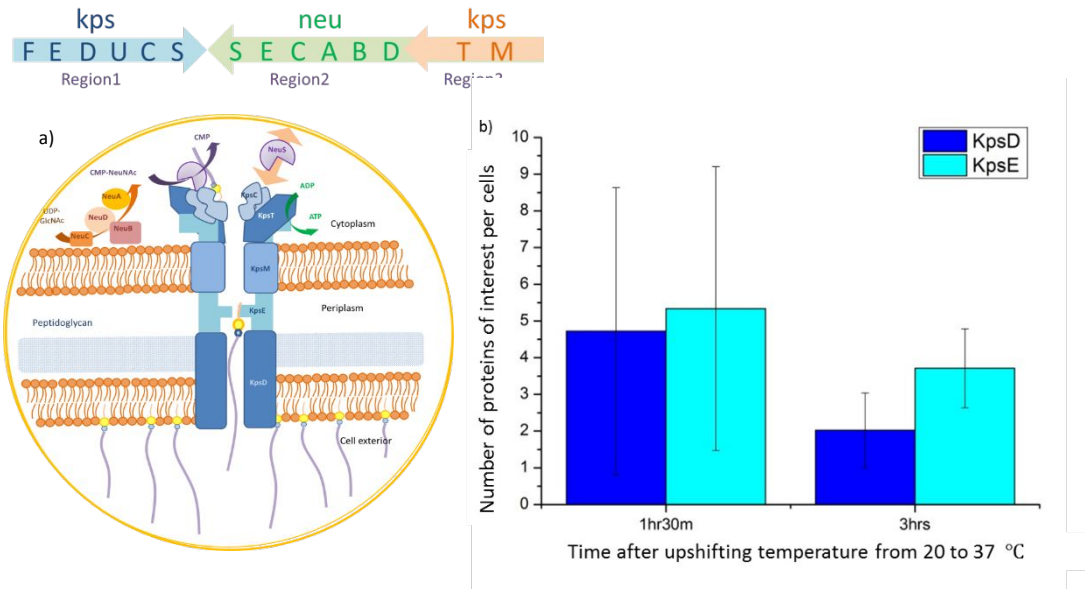

Figure S6. a) Schematic diagram showing the proteins and enzymes involved in bacterial capsular brush synthesis and transport from the highlighted operon regions. b) The number of labelled KpsD and KpsE at different time points from immuno labelling combined with fluorescence microscopy. These capsule synthesis proteins were up regulated when the bacterial cells when the temperature was upregulated from 20 to 37°C.

The function of capsular proteins expressed from the gene clusters (**Figure S6a**) in region 1 and region 3 is to support the translocation of K1 polysaccharides through the ABC transporter (the KpsMT complex[9-11]). However, the function of other capsular proteins involved in this activity is not yet clear, such as KpsS and NeuE. Enzymes encoded in region 2 behave as polymerases for the creation of the polysaccharides[12]. Although there are only a few essential enzymes in the polysialic synthesis process, e.g. NeuCBAS, the clarification of their roles and the interactions of these enzymes with others are still questioned. A better understanding of the role of NeuS would provide a much better picture of the activity of the whole biosynthesis pathway.

In **figure S6b**, the number of proteins per cell is shown: KpsD and KpsE after up regulation by the shift in temperature to 37 °C. The number of these complexes relates to the probability of the capsular brush rafts emerging on the bacterial surface.

References

1 Georgiades, P. *et al.* The flexibility and dynamics of the tubules in the endoplasmic reticulum. *Sci. Rep.* **7**, 1-10, doi:10.1038/s41598-017-16570-4 (2017).

2 Palayret, M. *et al.* Virtual-'light sheet' single-molecule localisation microscopy enables quantitative optical sectioning for super-resolution imaging. *Plos One* **10**, 1371, doi:10.1371/journal.pone.0125438 (2015).

3 Pincus, P. Colloid Stabilization with Grafted Polyelectrolytes. *Macromolecules* **24**, 2912-2919, doi:10.1021/ma00010a043 (1991).

4 Ma, H., Irudayanathan, F. J., Jiang, W. & Nangia, S. Simulating Gram-Negative Bacterial Outer Membrane: A Coarse Grain Model. *J. Phys. Chem. B* **119**, doi:10.1021/acs.jpcb.5b07122 (2015).

5 Pelkonen, S., Häyrinen, J. & Finne, J. Polyacrylamide gel electrophoresis of the capsular polysaccharides of Escherichia coli K1 and other bacteria. *J. Bacteriol.* **170**, 2646–2653, doi:10.1002/2014GB005021 (1988).

6 Vimr., S. M. S. a. E. R. Chromatographic Analysis of the Escherichia coli Polysialic Acid Capsule. *Methods Mol. Biol.* **966**, 109-120, doi:10.1007/978-1-62703-245-2_7 (2013).

7 Toikka, J., Aalto, J., Hayrinen, J., Pelliniemi, L. J. & Finne, J. The polysialic acid units of the neural cell adhesion molecule N-CAM form filament bundle networks. *J. Biol. Chem.* **273**, 28557–28559, doi:10.1074/jbc.273.44.28557 (1998).

8 Nahidiazar, L., Agronskaia, A., Broertjes, J., van den Broek, B. & Jalink, K. Optimizing Imaging Conditions for Demanding Multi-Color Super Resolution Localization Microscopy. *PLOS ONE* **11**, e0158884., doi:10.1371/journal.pone.0158884 (2016).

9 Rowe, S., Hodson, N., Griffiths, G. & Roberts, I. S. Regulation of the Escherichia coli K5 capsule gene cluster: Evidence for the roles of H-NS, BipA, and integration host factor in regulation of group 2 capsule gene clusters in pathogenic E. coli. *J. Bacteriol.* **182**, 2741-2745, doi:10.1128/JB.182.10.2741-2745.2000 (2000).

10 Cuthbertson, L., Kos, V. & Whitfield, C. ABC transporters involved in export of cell surface glycoconjugates. . *Microbiol. Mol. Biol. Rev.* **74**, 341-362, doi:10.1128/MMBR.00009-10 (2010).

11 Willis, L. M. & Whitfield, C. Structure, biosynthesis, and function of bacterial capsular polysaccharides synthesized by ABC transporter-dependent pathways. . *Carbohydr. Res.* **378**, 35-44, doi:10.1016/j.carres.2013.05.007 (2013).

12 Vimr, E. R. & Steenbergen, S. M. Early molecular-recognition events in the synthesis and export of group 2 capsular polysaccharides. *Microbiology* **155**, 9-15, doi:10.1099/mic.0.023564-0 (2009).